ADVANCING EARTH AND SPACE SCIENCE

JGR Atmospheres

RESEARCH ARTICLE
10.1029/2020JD032669

Statistical Reconstruction of Seasonal Tropical Cyclone Variability in the North Atlantic Basin

Matthew Lee Titus[1,2], **Keith R. Thompson**[3], **Eric C. J. Oliver**[3], **and Philip J. Klotzbach**[4]

[1]Environment and Climate Change Canada, Dartmouth, NS, Canada, [2]Department of Physics and Atmospheric Science, Dalhousie University, Halifax, NS, Canada, [3]Department of Oceanography, Dalhousie University, Halifax, NS, Canada, [4]Colorado State University, Fort Collins, CO, USA

Key Points:

- Relationship between North Atlantic tropical cyclone activity and concurrent mean sea level pressure is studied with redundancy analysis
- Primary redundancy index is physically interpreted in terms of overall tropical cyclone activity with ~50% variance explained from 1948 to 2016
- Secondary redundancy index is physically interpreted in terms of steering of storm tracks toward the coast of North America

Correspondence to:
M. L. Titus,
Lee.Titus@canada.ca

Citation:
Titus, M. L., Thompson, K. R., Oliver, E. C. J., & Klotzbach, P. J. (2021). Statistical reconstruction of seasonal tropical cyclone variability in the North Atlantic basin. *Journal of Geophysical Research: Atmospheres*, *126*, e2020JD032669. https://doi.org/10.1029/2020JD032669

Received 24 FEB 2020
Accepted 11 DEC 2020

Author Contributions:
Conceptualization: Matthew Lee Titus, Keith R. Thompson
Writing – original draft: Matthew Lee Titus, Keith R. Thompson, Eric C. J. Oliver, Philip J. Klotzbach
Writing – review & editing: Matthew Lee Titus, Keith R. Thompson, Eric C. J. Oliver, Philip J. Klotzbach

Abstract Seasonal forecasting of tropical cyclones is a topic of considerable interest to the public, government and private sectors. To improve understanding of the dynamics controlling the predictability of tropical cyclone (TC) activity, and improve the accuracy of forecasts, multiple studies have related TC activity to empirically-defined indices including the El Niño-Southern Oscillation, the Atlantic Multidecadal Oscillation, and the North Atlantic Oscillation. These indices were not developed to forecast TC activity but rather summarize other aspects of atmosphere-ocean variability. In this study we use a statistical approach, based on redundancy analysis, to define two indices related to overall activity and steering of TCs. We focus on North Atlantic TCs that reached tropical storm strength (≥34 kt) between August and October 1948–2016. TC occurrences are binned using an equal area grid that covers the North Atlantic. The redundancy indices are linear combinations of mean sea level pressure for the same season. Cross validation is used to guard against over fitting in the definition of the indices. This approach provides two physically interpretable redundancy indices related to North Atlantic TC activity. The leading redundancy index is used to successfully reconstruct the total number of TCs and the accumulated cyclone energy, over the extended period 1878–2014 using seasonal mean sea level pressures from the National Centers for Environmental Prediction 20th-Century Reanalysis version 2c. Extensions of the approach for seasonal forecasting are discussed.

1. Introduction

Tropical cyclones can cause major loss of life and have devastating impacts on infrastructure and transportation. The North Atlantic exhibits the highest variability of tropical cyclone (TC) activity of any ocean basin (Gray & Klotzbach, 2014) and the associated damages exhibit significant variability on interannual and longer timescales (Landsea, 2015; Pielke & Landsea, 1998). The recent upward trend in TC activity in the North Atlantic basin (Emanuel, 2005; Goldenberg et al., 2001; Kunkel et al., 2013) increases the need for accurate seasonal forecasts. While such forecasts currently show skill with regard to overall activity, they are presently of limited practical use due to lack of regionalization (Caron et al., 2020).

Various methods have been used to seasonally forecast TC activity. Statistical forecasts have the longest history and have been issued in real-time by Colorado State University, for example, since 1984 (Gray, 1984, 1984b; Klotzbach & Gray, 2009). These statistical forecasts are still used today and have exhibited modest improvement over time (Klotzbach et al., 2017). As computing power increased, dynamical seasonal TC forecasting began in Europe (Vitart et al., 2007) and was quickly followed by the United States (Camargo & Barnston, 2009). Hybrid statistical-dynamical models have also been developed (Vecchi et al., 2011).

Canada is affected by about one-third of the TCs that form in the North Atlantic basin. These TCs can either remain tropical or undergo extratropical transition by the time they impact Canada. Storms that have caused major impacts in Canada include Hazel (1954), Juan (2003), Igor (2010), and Dorian (2019). In this study, we focus on reconstructing historical TC variability as a step toward building a Canadian TC seasonal forecasting capability.

Xie et al. (2005) identified several spatio-temporal modes of hurricane activity in the North Atlantic (20°–50°N, 50°–86°W) based on empirical orthogonal function analysis. The two dominant modes accounted for over 40% of the total variance. The modes represent (1) the overall level of hurricane track density in the study region and (2) zonal shifts in hurricane tracks. Overall, hurricane activity was found to be statistically related to the Atlantic Sea Surface Temperature (SST) dipole mode, El Niño-Southern Oscillation (ENSO) and vertical wind shear over the main development region. The zonal shift in hurricane tracks was found to be most highly correlated with the Atlantic SST dipole mode and the North Atlantic Oscillation (NAO).

Mei et al. (2014) performed a modeling study of interannual and decadal variability of TC track density over the North Atlantic for the period 1979 and 2008. The study used simulations by the High Resolution Atmospheric Model (HiRAM) forced by observed SST. A basin-wide mode of TC track density was found to dominate on both interannual and decadal timescales. On interannual timescales, the mode was controlled by SST over the central eastern equatorial Pacific and the tropical North Atlantic. On decadal timescales, the mode was related to the difference in SST between the tropical North Atlantic and Northeast Pacific, and the difference between the tropical North and South Atlantic.

Colbert and Soden (2012) investigated the relationship between TC tracks and large-scale steering parameters for the North Atlantic basin over the period 1950–2010. Only TCs that formed in the main development region were considered. Three track types were identified: straight moving, recurving landfall, and recurving ocean. They found that recurving ocean storms were associated with a weakened subtropical ridge whereas straight moving storms were associated with a westward-extended and relatively strong ridge. Colbert and Soden (2012) argued that anomalously warm ENSO conditions led to a weakening of the subtropical ridge and a higher percentage of recurving ocean storms.

Gray (1984, 1984b) was the first of many (e.g., Colbert & Soden, 2012; Kossin et al., 2010; Xie et al., 2005) to relate North Atlantic TC variability to ENSO. North Atlantic TC variability has also been related to the NAO (e.g., Colbert & Soden, 2012; Kossin et al., 2010; Xie et al., 2005), and many other environmental indices (e.g., Colbert & Soden, 2012; Elsner et al., 2000; Gray, 1984, 1984b; Hart, 2011; Kossin et al., 2010; Landsea et al., 1994; Xie et al., 2005). The NAO, and ENSO-related indices such as Nino 3.4 and the Southern Oscillation Index (SOI), were not developed to reconstruct TC activity directly but rather to summarize other aspects of atmosphere-ocean variability. It follows there is no guarantee that these indices are "fit for purpose".

In this study we use, for the first time, a statistical technique called redundancy analysis (e.g., Bakalian et al., 2010; Tyler, 1982; von Storch & Zwiers, 2002) to construct indices that are designed to predict TC variability in the North Atlantic basin. Note we are using "predict" here in the statistical sense of predicting a set of response variables from a set of independent variables (e.g., Johnson et al., 2002). We use the word "forecast" for prediction of future seasonal mean states of the atmosphere. The leading redundancy indices are also physically interpreted in terms of dynamical processes known to be related to TC dynamics.

Based on the above studies and others (Brennan, 1935; Fogarty & Gyakum, 2005; Knaff, 1997; Landsea et al., 1999; Ray, 1935), we focus on reconstructing TC variability from concurrent gridded fields of mean sea level pressure (MSLP). We identify two statistically significant redundancy modes that are connected to TC activity. The first mode describes overall TC activity in the North Atlantic and is related to the strength of the low-level trade winds across the western subtropical Atlantic as well as the strength and westward extension of the subtropical ridge. The second mode describes a zonal shift in TC tracks and is related to the MSLP difference along the east coast of North America and the strength of the subtropical high in the southeastern North Atlantic. We show that the first mode can reconstruct yearly changes in overall TC activity from 1878 to 2014 with at least as much skill as other commonly used indices.

The structure of the paper is as follows. The data and its preprocessing are described in Section 2. This is followed in Section 3 by an overview of the statistical methodology used to relate TC occurrences to MSLP. In Section 4, the dominant spatial patterns, and their time-varying amplitudes, are physically interpreted. In Section 5, we use a different reanalysis dataset to reconstruct TC activity over the extended period from 1878 to 2014. The results, and plans for seasonal forecasting of TC occurrences, are summarized in Section 6.

2. Data and Preliminary Analysis

2.1. Tropical Cyclone Occurrences

The HURDAT2 database (Landsea & Franklin, 2013) contains the intensity and location of all North Atlantic TCs and subtropical cyclones with a time step of 6 hours from 1851 to near present time. In this study

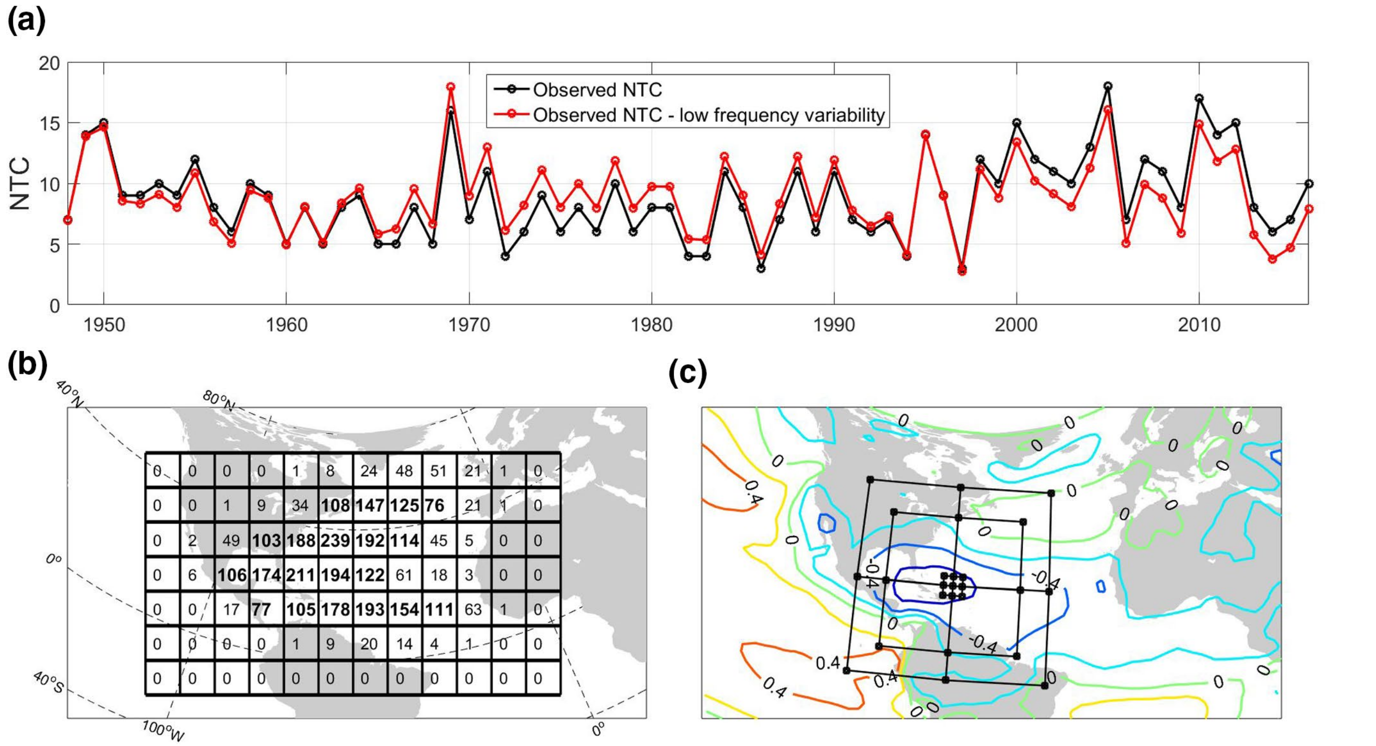

Figure 1. (a) Time series of the total number of tropical cyclones (NTC) from 1948 to 2016 before (black) and after (red) removal of its low frequency component (see Section 2.1 for details). (b) The grid used to calculate TC occurrences over the North Atlantic. The numbers show the total TC occurrences for each grid cell from 1948 to 2016. The 20 grid cells with bold black text have totals greater than or equal to 70. (c) Correlation of seasonal MSLP and NTC based on observations from 1948 to 2016. Contour interval is 0.2. The 3×3 pressure predictor grids for sets 1, 7, and 10 (see Table 1) are also shown. Grids are centered on the location of the strongest sample correlation between MSLP and NTC ($\hat{\rho} = -0.65$ at 22.6°N, 67.5°W).

we focus on storms that met the following criteria: (i) occurred between 1948 and 2016, (ii) reached tropical storm strength (1-min sustained winds $\geq$ 34 kt), and (iii) first observed in August, September, or October (ASO). No criteria related to dynamical structure were used and so subtropical and extratropical stages are included. We include extratropical stages of TCs because many significant storms impacting Canada were formerly TCs that had just become extratropical (e.g., Dorian 2019).

We first calculated the total number of TCs (NTC) for each year subject to the above selection criteria. Low frequency variability is clearly evident (Figure 1a). Cross spectral analysis (not shown) indicated a statistically significant relationship between NTC and the ASO-averaged Atlantic Multidecadal Oscillation (AMO) index at low frequencies. To remove low frequency variability from the NTC time series, the seasonal AMO index was first smoothed with a 10 year running average. The NTC was then regressed on the low frequency AMO and a linear trend. The residual from this multiple regression is taken to be the high frequency component of NTC and is shown by the red line in Figure 1a.

To examine the spatial structure of TC activity, a grid was defined over the North Atlantic using an Albers equal area projection (Snyder, 1987). This projection was used to ensure that the grid cells have approximately the same area (Figure 1b). To calculate the occurrences for the grid cells, each TC track was linearly interpolated from a time spacing of 6 h down to 15 min. The interpolation was done to avoid missing occurrences for faster moving TCs, or TCs that passed close by corners of grid cells. We tried a number of time spacings and found a decrease in time spacing below 15 min did not change the total occurrences assigned to each grid cell. A TC was counted if it moved into a grid cell regardless of its strength at the time of entry. The only way a TC could be counted more than once would be if it left the grid cell and re-entered at a later time.

Figure 1b shows the total occurrences for each grid cell over the period 1948–2016. Grid cells with total occurrences below 70 were removed in order to focus on regions with relatively high TC activity. The low

Table 1
Approximate Grid Spacing for the Ten MSLP Predictor Sets

Predictor set	Grid spacing, Δ (km)
1	320
2	640
3	960
4	1290
5	1620
6	1950
7	2290
8	2630
9	2980
10	3330

Note. Each predictor set contains nine MSLP time series defined on a 3 × 3 grid. The grids for predictor sets 1, 7, and 10 are plotted in Figure 1c.

frequency variability of the individual TC occurrence time series, for the 20 grid cells shown in Figure 1b, was removed using the same method applied to the NTC time series.

The quality of the TC data varies with time. This is largely the result of better monitoring of mesoscale variability by aircraft reconnaissance (beginning in the mid-1940s) followed by satellite sensing (beginning in the mid-1960s). One way to allow for these changes in the observing system is to correct the observations for the early undercounting (Vecchi & Knutson, 2008) and the more recent increase in short-lived storms (Landsea et al., 2010; Villarini et al., 2011). An alternative approach is to remove the low frequency variability from the TC data. We have chosen the latter approach in the present study. The effect of removing low frequency variability is discussed in Section 5.

2.2. Mean Sea Level Pressure

Gridded fields of monthly MSLP for 1948–2016 were obtained from the NCEP/NCAR Reanalysis 1 (Kalnay et al., 1996). The fields are global with a grid spacing of 2.5° in latitude and longitude. Seasonal ASO means were first calculated for each year. The correlation between seasonal MSLP and NTC, after removal of linear trends, is shown in Figure 1c. The strongest correlation is found just east of the Bahamas ($\hat{\rho} = -0.65$, P-value < 0.001 allowing for autocorrelation).

We next defined a set of 10 nested grids (Table 1), each with 3×3 grid points, centered on the location of the strongest correlation. The grids were defined on an Albers equal area projection. Three of the grids are shown in Figure 1c. The reanalysis data were interpolated to each of the pressure grids using Delaunay triangulation of the reanalysis grid locations and linear interpolation over each triangle. The result is 10 sets of nine predictors for the TC occurrences. The low frequency variability of each MSLP grid point time series was removed using the same method applied to the NTC time series (Section 2.1).

3. Optimal Model Estimation

We now describe the method used to statistically predict the gridded TC occurrences for a given season from the concurrent gridded MSLP. The theoretical background is given in the Appendix.

We start by assuming the observed seasonal TC occurrences for year index t are stored in the $q \times 1$ vector y_t where q is the number of TC occurrence grid cells. In the present study $q = 20$ (the number of grid cells with at least 70 storms shown in bold text in Figure 1b). The observed seasonal MSLP is specified on a 3×3 grid (see Figure 1c for three of the predictor grids). The MSLP values are stored in the $p \times 1$ vector x_t where p is the number of predictors. In the present study $p = 9$.

Our goal is to predict y_t from x_t using a linear model with parameters estimated from $n = 69$ multivariate observations of (x_t, y_t) from the period 1948 to 2016. Note the mean of each observed time series was removed prior to analysis as part of the high pass filtering described in Section 2.1. At first sight it would appear the predictions could be based on a multivariate regression of y_t on x_t. Unfortunately, the number of regression coefficients is large ($pq = 180$), and the MSLP predictors are highly correlated. This results in a multivariate regression model that is difficult to interpret physically, and highly sensitive to small changes in individual values of MSLP.

Our approach is to use a modified form of redundancy analysis to predict y_t from x_t. (Details are given in the Appendix.) The prediction is of the form

$$\hat{y}_t = e_1 a_1' x_t + e_2 a_2' x_t + \ldots e_r a_r' x_t \tag{1}$$

where the e_i are (orthonormal) column vectors of length q defined on the TC occurrence grid, and the a_i' are row vectors of length p defined on the MSLP grid.

The interpretation of this model is straightforward. Consider the case $r = 1$. To predict y_t first calculate the inner product of x_t and a_1. This gives the first redundancy index

$$R_{1t} = a_1' x_t \tag{2}$$

where subscript t highlights the dependence of this scalar quantity on time. To predict y_t we multiply the redundancy index by the spatial pattern e_1:

$$\hat{y}_t = e_1 R_{1t}$$

The extension to $r > 1$ is straightforward and involves additional spatial patterns defined on the TC occurrence grid and redundancy indices:

$$\hat{y}_t = e_1 R_{1t} + e_2 R_{2t} + \ldots e_r R_{rt} \tag{3}$$

The estimation of $\{e_i, R_{it} | i = 1, \ldots r, t = 1, \ldots n\}$ is based on the equations given in the Appendix with population covariances replaced by sample covariances. The e_i and R_{it} depend on (i) the predictor set (equivalently Δ, see Table 1) (ii) the "ridge" parameter α^2, and (iii) the number of redundancy predictors r. We chose Δ, α^2 and r based on cross validation (e.g., Hastie et al., 2009). This involved fitting the model over multiple training sets and minimizing the square prediction error summed over the corresponding validation sets. To illustrate, for "leave-one-out" cross validation we minimize

$$\gamma^2(\Delta, \alpha^2, r) = \frac{\sum_{t=1}^{n} (y_t - \hat{y}_t)' (y_t - \hat{y}_t)}{\sum_{t=1}^{n} y_t' \, y_t} \tag{4}$$

where $\hat{y}_t$ is the vector of predicted TC occurrences for time t based on fitting the model to observations for times 1, ..., $t - 1$, $t + 1$, ...n.

To illustrate the approach, Figure 2 shows plots of γ^2 as a function of α for six MSLP predictor sets. The three lines in each panel correspond to $r = 1$, 2, and 9 redundancy predictors, see (3). All γ^2 curves are qualitatively similar with (i) a single minimum for α between about 0.3 and 0.6 hPa, and (ii) $\gamma^2 \to 1$ as $\alpha \to \infty$. (This latter feature is to be expected as explained in the Appendix.) The use of $r = 2$ redundancy predictors generally outperforms models based on a single predictor. It also performs almost as well as, or in some cases better than, ridge regression which uses $r = 9$ predictors. The reason the $r = 2$ model can outperform the $r = 9$ model is that cross validation is used to assess model performance, thereby allowing for the possibility of overfitting. As a result, including more redundancy predictors (increasing r) does not necessarily increase model skill as measured by γ^2.

The optimal model takes the form

$$\hat{y}_t = e_1 a_1' x_t + e_2 a_2' x_t \tag{5}$$

Each term on the right-hand side of this equation involves three components: a spatial pattern defined on the TC occurrence grid (e_1, e_2), a spatial pattern defined on the pressure grid (a_1, a_2), and the time varying MSLP (x_t) defined on the 3×3 pressure grid. Based on Figure 2, we choose predictor set seven for the optimal model. The latitudes and longitudes of this predictor grid are given in Table 2 and plotted in Figure 1c. The associated value of $\Delta = 2{,}290$ km (Table 1) is the optimal pressure grid spacing for calculating linear gradients, and curvature of the pressure surface, for predicting TC occurrences. The optimal model is further defined by taking $\alpha = 0.36$ hPa (see bottom left panel of Figure 2).

The optimal model, fit to the complete record from 1948 to 2016, accounts for 85% of the total variance of the TC occurrences that can be predicted by MSLP, that is, $(\lambda_1 + \lambda_2)/(\lambda_1 + \ldots \lambda_p)$, see Appendix. It is important to note that sum of squared prediction errors, $\sum_{t=1}^{n} (y_t - \hat{y}_t)' (y_t - \hat{y}_t)$, is 79% of the total sum of squared TC occurrences, $\sum_{t=1}^{n} y_t' \, y_t$. This implies that most of the variability of the TC occurrences cannot be

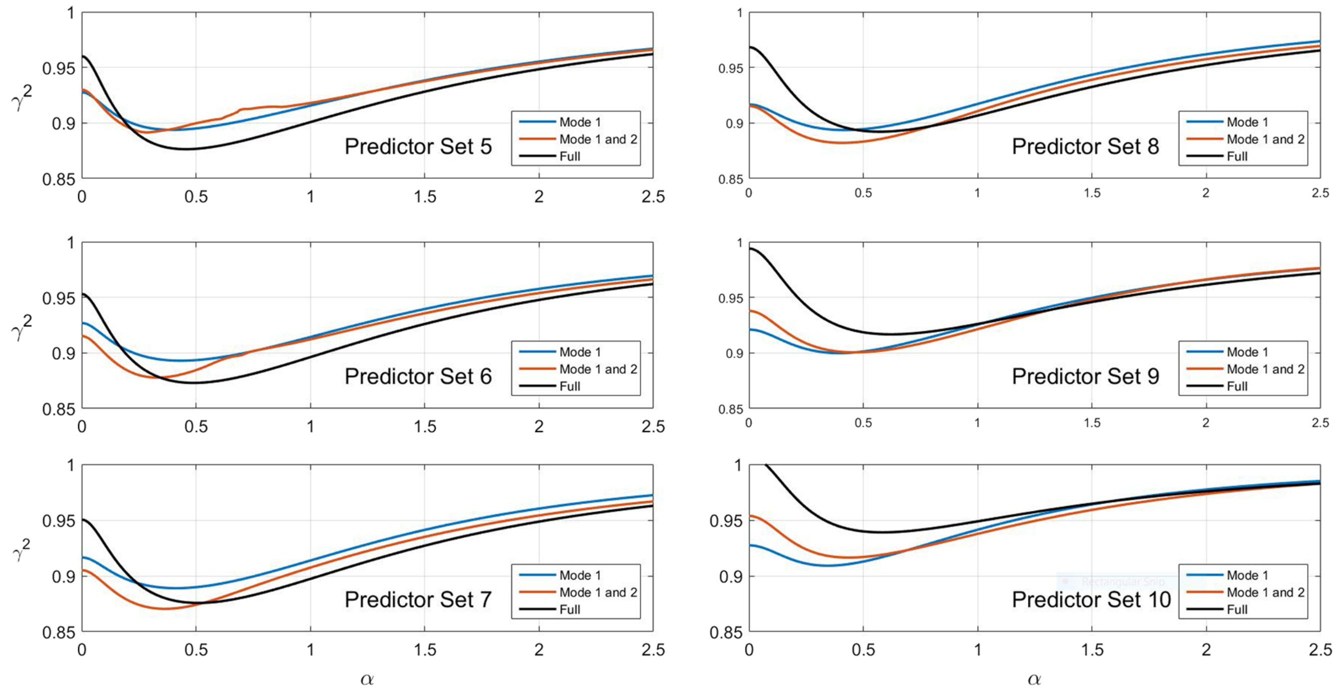

Figure 2. Defining the optimal model using "leave-one-out" cross validation. Each subplot shows, for a given predictor set, the normalized mean squared prediction error (γ^2, see [4]) as a function of the square root of the ridge parameter, α. The three lines in each panel correspond to the use of $r = 1$, 2 and 9 redundancy predictors.

predicted by MSLP. We show in the next section that the optimal model is most effective at predicting the large-scale variability of TC occurrences.

4. Physical Interpretation of the Optimal Model

4.1. Redundancy Mode 1 (Activity Index)

The three components of the first mode are plotted in the left panels of Figure 3. The pattern on the TC occurrence grid (e_1, Figure 3a) has positive weights for all grid cells. It is also similar to the climatology of TC occurrences shown in Figure 1b. R_{1t} can be interpreted in terms of overall TC activity. When R_{1t} is positive, the first mode implies higher TC activity over the whole North Atlantic; when the index is negative, below-average TC activity is expected. This relationship is supported by the positive correlation ($\hat{\rho} = 0.69$) between R_{1t} (Figure 3c) and the NTC time series (Figure 1a). We will henceforth refer to R_{1t} as the Activity Index.

Figure 4 provides some insights into the underlying physics of the first mode. The correlation of the Activity Index with the gridded MSLP time series is negative across the subtropical Atlantic (Figure 4a). Consistent with Gray (1984, 1984b), TC activity is negatively correlated with MSLP in this region, implying a strong subtropical ridge is associated with fewer Atlantic TCs in a given hurricane season.

In addition to the negative correlation of the Activity Index with MSLP across the subtropical Atlantic, Figure 4a also shows a positive correlation over the equatorial Pacific. Thus when the Activity Index is high, we should also expect a relatively weak pressure gradient between the equatorial Pacific and the subtropical Atlantic that will weaken the easterly trade winds across the tropical Atlantic. This is consistent with the correlation between the Activity Index and the seasonal mean zonal wind at 925 hPa extracted from the reanalysis (Figure 4b).

Table 2
Latitude and Longitudes of the 3 × 3 Grid for MSLP Predictor Set 7 (See Figure 1c). p_{ij} Refers to Pressure on Row i and Column j of the Predictor Grid

p_{11} (41.3°N 92.5°W)	p_{12} (43.3°N 67.9°W)	p_{13} (42.1°N 43.1°W)
p_{21} (21.0°N 89.0°W)	p_{22} (22.6°N 67.5°W)	p_{23} (21.6°N 45.9°W)
p_{31} (0.8°N 86.3°W)	p_{32} (2.3°N 67.2°W)	p_{33} (1.3°N 48.1°W)

Figures 4a and 4b together suggest that the Activity Index is related to the zonal trade winds over the tropical Atlantic. This is consistent with the study of Saunders et al. (2017) who found that the 950 hPa zonal wind

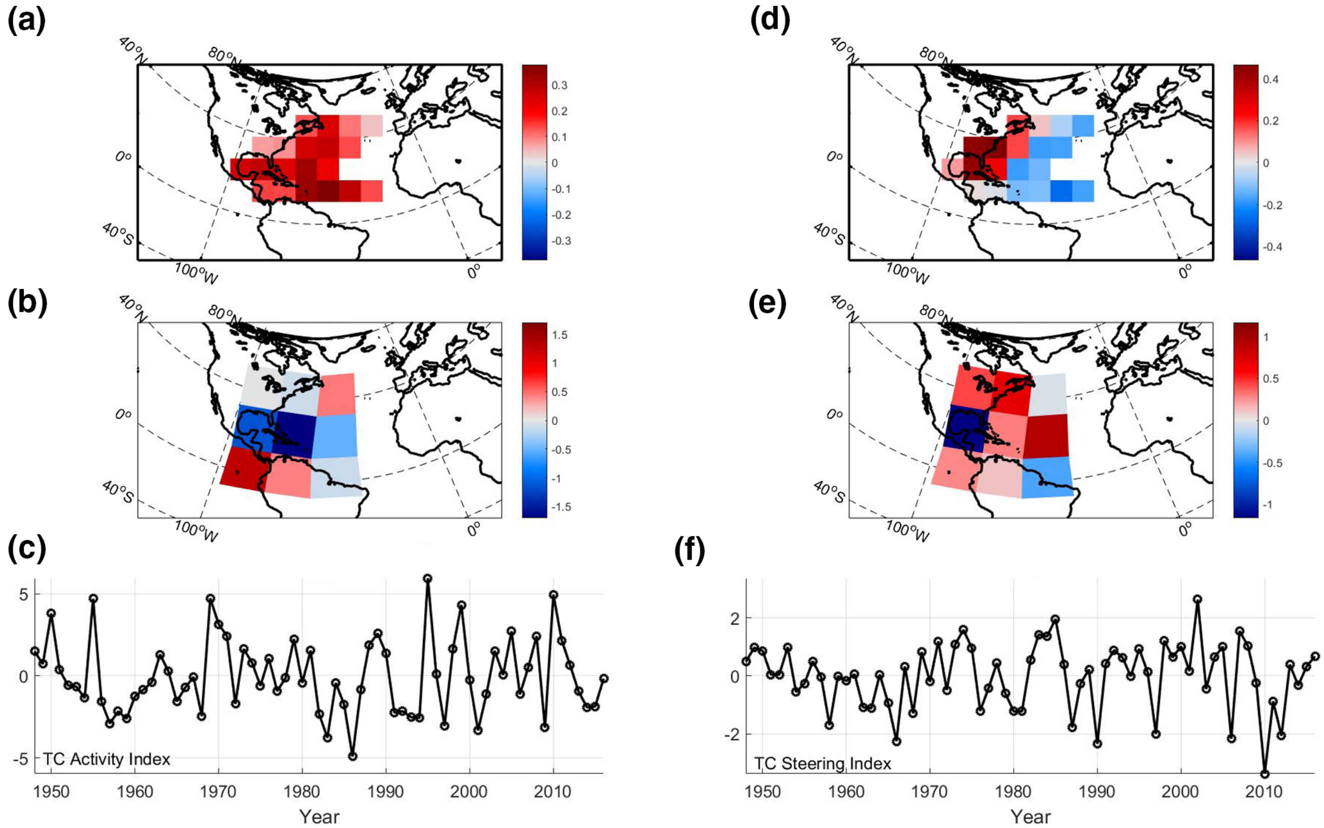

Figure 3. The first two redundancy modes. Panels (a), (b), and (c) show the spatial patterns and time varying index for the first mode (e_1, a_1 and the Activity Index respectively). Mode e_1 is defined on the TC occurrence grid and a_1 is defined on the pressure grid. Panels (d), (e), and (f) are the corresponding plots for the second redundancy mode (e_2, a_2 and the Steering Index respectively).

over the tropical Atlantic, for the period 1878–2012, was the most skillful predictor of August-September hurricane activity ($\hat{\rho}$ = 0.67). Given anomalous westerly flow at low levels, the trade winds are weaker than normal, typically resulting in more Atlantic TCs. There are several likely reasons for this observed relationship. First, weaker low-level trades are generally associated with less vertical wind shear, given that upper-level winds in the tropical Atlantic and Caribbean are typically westerly. Weaker vertical wind shear is well known to be a necessary condition for hurricane formation and maintenance (DeMaria, 1996; Gray, 1968; Jones et al., 2020; Knaff et al., 2004). Weaker trade winds are also associated with increased low-level cyclonic vorticity (Klotzbach, 2011; Saunders & Lea, 2008; Saunders et al., 2017, 2020) in the tropical Atlantic and Caribbean, helping to spin up developing TCs. Weaker trades are also consistent with higher pressure in the eastern equatorial Pacific and lower pressure in the tropical Atlantic (Saunders & Lea, 2008; Saunders et al., 2020). Higher pressure in the eastern equatorial Pacific is associated with a positive SOI and typically La Niña conditions (Power & Kociuba, 2011). Low pressure in the tropical Atlantic is typically associated with warmer than normal sea surface temperatures and a more unstable atmosphere, both of which favor TC formation and intensification (Klotzbach, 2007; Klotzbach et al., 2018).

The four correlation maps shown in Figure 4 are only being used to interpret the two redundancy indices. By construction, the redundancy indices are linear combinations of MSLP and, through the geostrophic relationship, are also expected to be correlated with the wind field. For this reason, we have not attempted to identify regions on these maps with statistically significant correlations.

Based on the above physically-motivated discussion, and examination of the a_1 weights (Table 3), we propose the following simplified Activity Index:

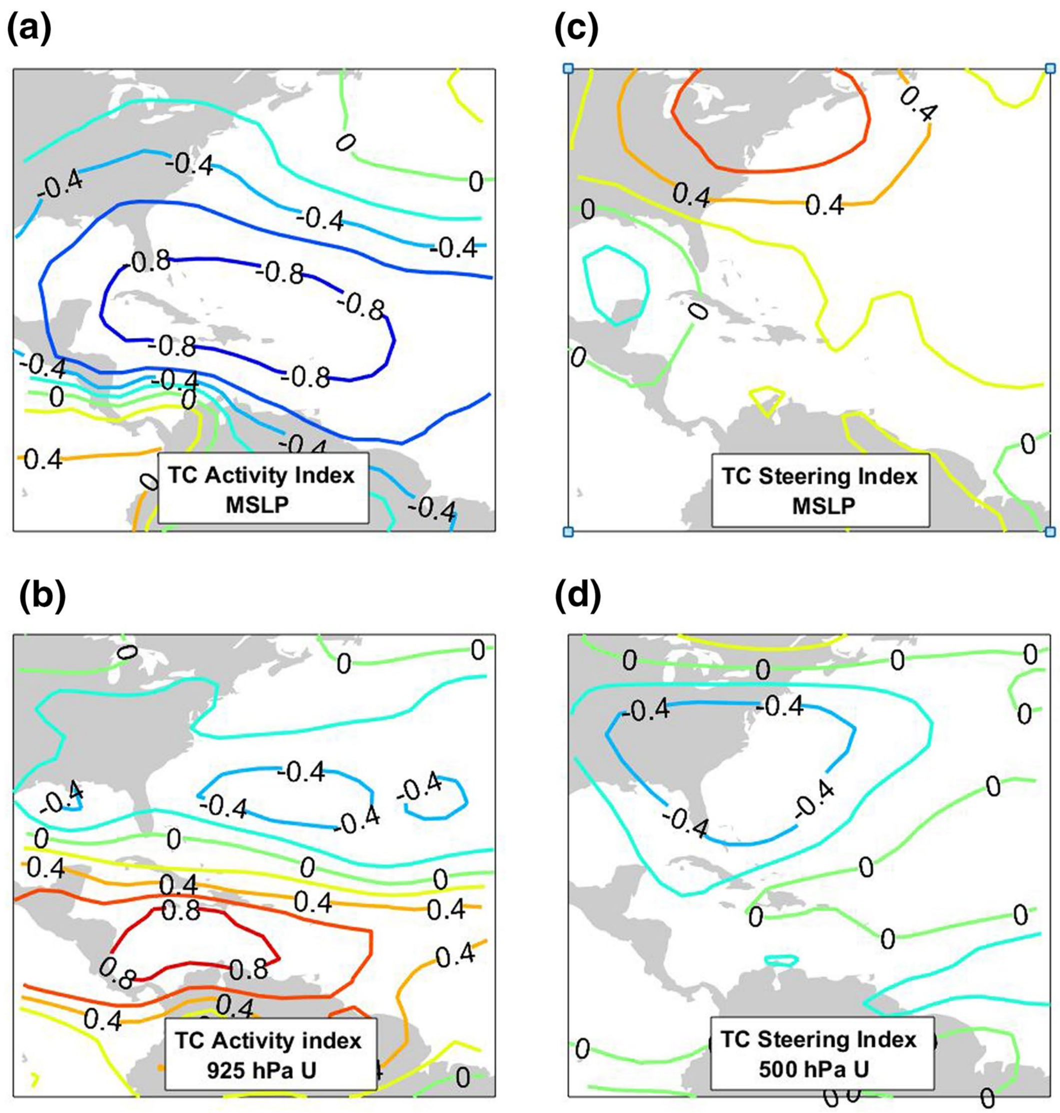

Figure 4. Correlation of the first two redundancy indices (Activity Index and Steering Index) with seasonal MSLP, and zonal wind for the period 1948–2016. The left column shows the correlation of the Activity Index with (a) MSLP and (b) zonal wind at 925 hPa. The right column shows correlations of the Steering Index with (c) MSLP and (d) zonal wind at 500 hPa.

$$\tilde{R}_{1t} = \underbrace{p_{31} - p_{22}}_{(I)} - \underbrace{(p_{21} + p_{22})\,/\,2}_{(II)} \tag{6}$$

Table 3
Elements of the Vectors a_1 and a_2 Used to Define the First Two Redundancy Indices for the Optimal Model

p_{ij}			a_1			a_2		
p_{11}	p_{12}	p_{13}	−0.01	−0.10	0.45	0.42	0.70	−0.03
p_{21}	p_{22}	p_{23}	−1.14	−1.70	−0.52	−1.17	0.30	0.93
p_{31}	p_{32}	p_{33}	1.28	0.43	−0.12	0.28	0.11	−0.41

Note. The p_{ij} refer to locations of the predictor set seven pressure grid shown in Figure 1c. a_1 and a_2 are plotted in Figure 3b and 3e.

where p_{ij} is the MSLP on row i and column j of the optimal predictor grid (see Table 2). This simplified index has a correlation of $\hat{\rho} = 0.97$ with the Activity Index. The simplified index can be interpreted as the sum of two contributions: (I) the pressure gradient across the western subtropical Atlantic that drives the near-surface zonal wind, and (II) the strength and westward extension of the subtropical ridge. High values of this index are associated with weaker near-surface zonal winds in the western subtropical Atlantic and lower pressure averaged over the Caribbean and Gulf of Mexico. Both of these contributions are correlated with more active

Atlantic hurricane seasons (Gray, 1984, 1984b; Saunders et al., 2020). We explore the usefulness of this simplified index when we reconstruct North Atlantic TC activity over the extended period 1878–2014 in Section 5.

4.2. Redundancy Mode 2 (Steering Index)

The three components of the second mode are plotted in the right panels of Figure 3. The pattern on the TC occurrence grid (e_2, Figure 3d) has positive weights near the coast of North America and negative weights further offshore. This means R_{2t} can be interpreted as a zonal shift of TC occurrences. When R_{2t} is positive, TCs are expected to be steered closer to the coast of North America; when the index is negative, recurvature of TCs away from the coast of North America is more likely. We will henceforth refer to R_{2t} as the Steering Index.

Figure 4c shows that the correlation between the Steering Index and MSLP is quite complex, but if the Steering Index is positive, MSLP increases to the northeast along the east coast of North America. This is consistent with the study of Fogarty and Gyakum (2005). The physical interpretation is that TCs closer to shore are associated with anomalous ridging over the northeast United States and eastern Canada driving TCs westward and inhibiting recurvature. Figure 4c also demonstrates that the Steering Index has a positive correlation with locations to the southeast of Atlantic Canada. This points to the influence of the strength of the subtropical high on recurvature, consistent with Colbert and Soden (2012). Figure 4d shows the correlation between the Steering Index and the seasonal zonal wind at 500 hPa, a proxy for the steering flow. When the Steering Index is high, the zonal wind is weaker than normal, and this is associated with reduced recurvature. Conversely, when the Steering Index is negative, the zonal wind is stronger than normal, leading to recurvature of TCs with fewer TCs approaching North America.

Based on the above physically-motivated discussion, and examination of the a_2 weights (Table 3), we propose the following simplified Steering Index:

$$\tilde{R}_{2t} = \underbrace{(p_{11} + p_{12})\,/\,2 - p_{21}}_{(I)} + \underbrace{p_{23}}_{(II)} \tag{7}$$

This simplified index has a correlation of $\hat{\rho} = 0.97$ with the Steering Index. The simplified index can be interpreted as the sum of two contributions: (*I*) the pressure gradient along coastal North America from the Gulf of Mexico to eastern Canada, and (*II*) the strength of the subtropical high in the North Atlantic. High values of this index are associated with anomalous high pressure over eastern Canada and anomalous low pressure over the Gulf of Mexico (Fogarty & Gyakum, 2005). High values of this index are also associated with a stronger subtropical high (Colbert & Soden, 2012).

To further physically interpret the steering mode, years were identified when the Steering Index was in the top third of all of its values, and years when it was in the bottom third. For each group of 23 years, the longitudes of storms crossing 35°N were estimated from the storm tracks obtained from HURDAT2. Histograms of the crossing longitudes of storms in "high" and "low" Steering Index years are shown in Figure 5. The crossing longitudes are approximately normally distributed for each group and have a range of roughly 80° of longitude. The histogram for high Steering Index years is shifted westward by about 6° longitude relative to low years, consistent with the above discussion of how the Steering Index is related to recurvature of TCs. The Wilcoxon rank sum test rejected, at the 1% level, the null hypothesis that the two distributions of crossing longitudes are the same, in favor of the alternative hypothesis that the two distributions are systematically shifted with respect to each other.

5. Historical Reconstructions

5.1. The Activity Index

We now assess how well the Activity Index, and its simplified form $\tilde{R}_{1t}$, can reconstruct variations of North Atlantic NTC and Accumulated Cyclone Energy (ACE, Bell et al., 2000) over the extended period 1878–

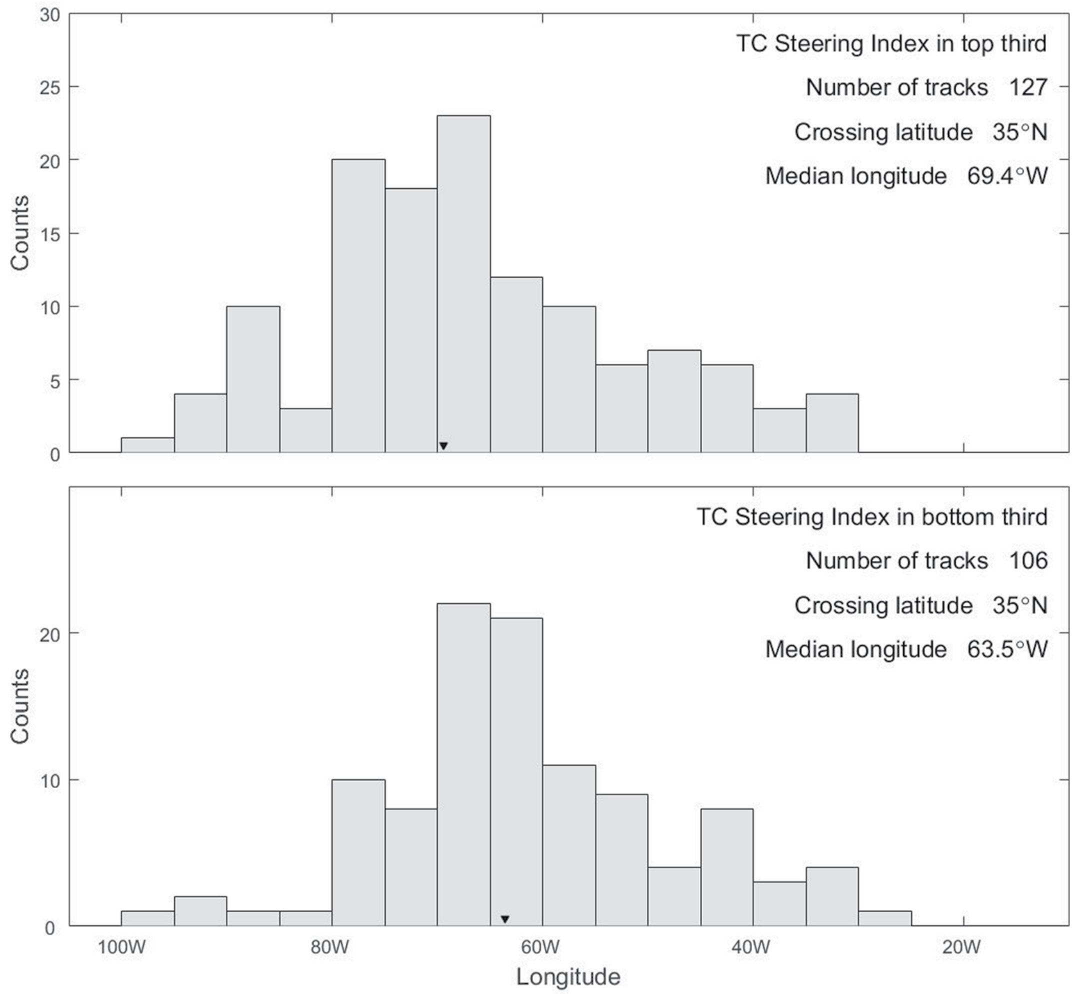

Figure 5. Histograms of the longitudes at which TCs crossed 35°N during ASO, 1948–2016. The upper panel is for years when the Steering Index was in the top third of all values. The lower panel is for years when the Steering Index was in the lower third of all values. The small triangles show the median crossing longitude for each group. The median value is also given in the upper right hand corner of each panel, along with the number of TC tracks for each group.

2014. We use MSLP from the National Centers for Environmental Prediction (NCEP) 20th Century Reanalysis version 2c (20CR, Compo et al., 2011) to reconstruct the Activity Index and $\tilde{R}_{1_t}$. One of the benefits of 20CR is that it includes estimates of the uncertainty of the reanalysis in the form of a 56-member ensemble. We extracted the complete MSLP ensemble for 1851–2014 and calculated 56 realizations of the Activity Index and $\tilde{R}_{1_t}$ by (i) averaging the 6-hourly MSLP fields to ASO seasonal means, and (ii) using the nine grid locations from 20CR that are nearest to predictor set 7 (Table 2). We then calculated the ensemble mean and standard deviation of the Activity Index and $\tilde{R}_{1_t}$ for each year. The ensemble standard deviation (not shown) was relatively constant from 1878 to 2014, but was noticeably higher before 1878, the year that the US Signal Service Corps started systematically tracking hurricanes (Saunders et al., 2017). We restrict the following analysis to the period 1878–2014. Low frequency variability was not removed from the MSLP, NTC or ACE time series prior to the following analysis.

We start by estimating correlations using a sliding window of length 31 years. The goal is to examine the time variation of the correlation of the ensemble mean Activity Index, and additional environmental indices, with NTC and ACE over the period 1878–2014. Each individual correlation is based on time series of length 31 years from which sample means have been removed. It follows that applying the sliding window effectively high-pass filters each input time series by removing a 31 year running mean.

10.1029/2020JD032669

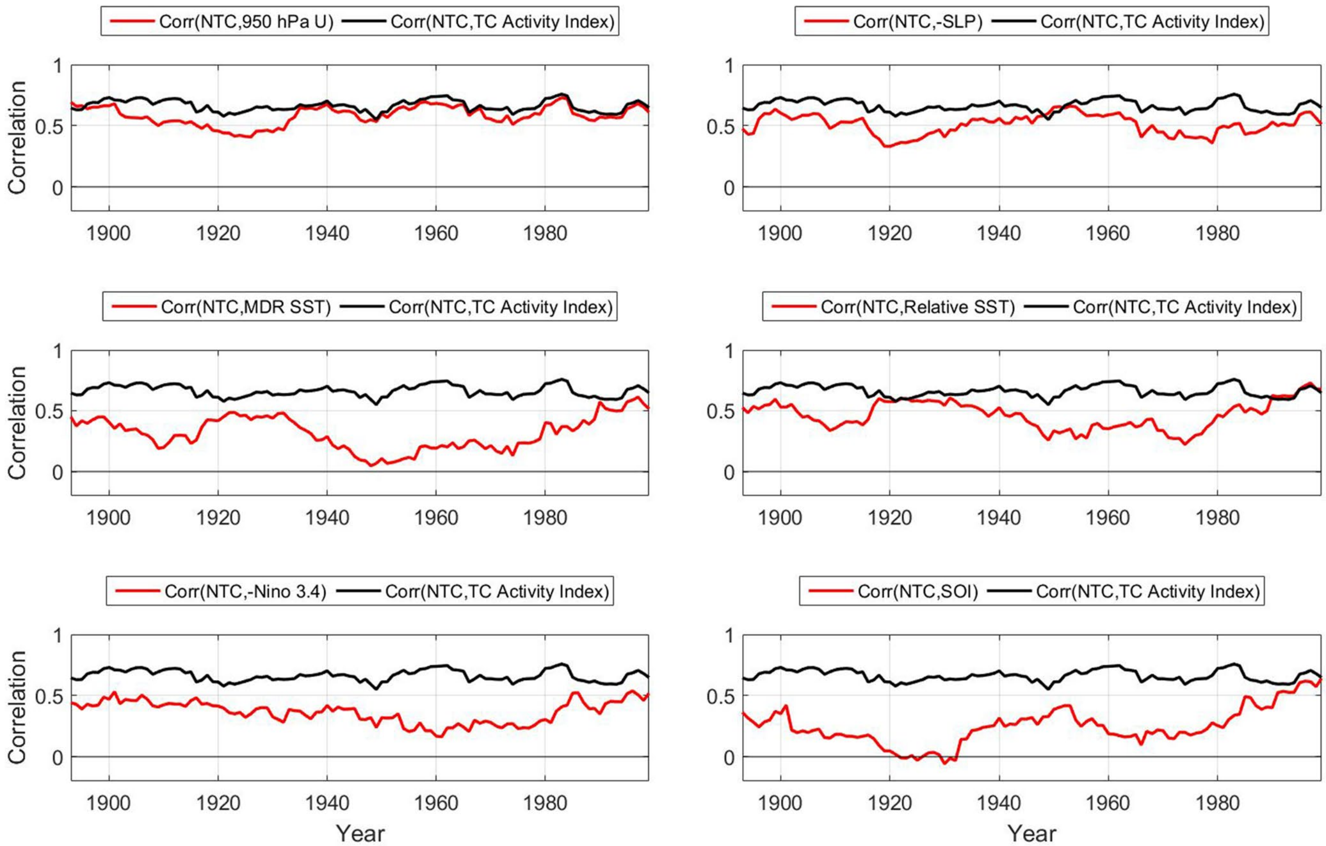

Figure 6. Time-varying correlations of NTC with the Activity Index and the six environmental indices listed in Table 4. A 31-year sliding window was used over the period 1878–2014. The time axis runs from 1893–1999 to exclude end effects of the sliding window. The black line (same in all panels) is the correlation between NTC and the Activity Index. The red line is the correlation between NTC and the environmental index given in the title of each panel.

The running correlation between the Activity Index and NTC has a relatively constant value of $\hat{\rho} \approx 0.7$ over the period 1878–2014 (black lines, Figure 6). For comparison, we found a correlation of $\hat{\rho} = 0.69$ for the period 1948–2016 (Section 4). The agreement is encouraging and indicates the Activity Index is not affected significantly by over fitting.

The running correlations between NTC and the six environmental indices of Saunders et al. (2017) are generally lower, and less stable, than the correlations of NTC and the Activity Index. Details of the six environmental indices are given in Table 4. We confirm the results of Saunders et al. (2017) that the most stable of the six indices is the 950 hPa zonal wind. We note however that the correlation between 950 hPa

Table 4
The Six Environmental Indices of Saunders et al. (2017)

Index	Averaging region and stations	Data source
950 hPa U	7.5–17.5°N, 100-30°W	20CRv2c
SLP	10-20°N, 60-20°W	20CRv2c
MDR SST	10-20°N, 60-20°W	NOAA ERSSTv5
Relative SST	10-25°N, 80-20°W minus 30°S-30°N, 0–360°	NOAA ERSSTv5
Nino 3.4 SST	5°S-5°N, 170-120°W	NOAA ERSSTv5
SOI	Tahiti minus Darwin MSLP	Australian Bureau of Meteorology

Abbreviations: NOAA, National Oceanic and Atmospheric Administration; SST, Sea Surface Temperature.

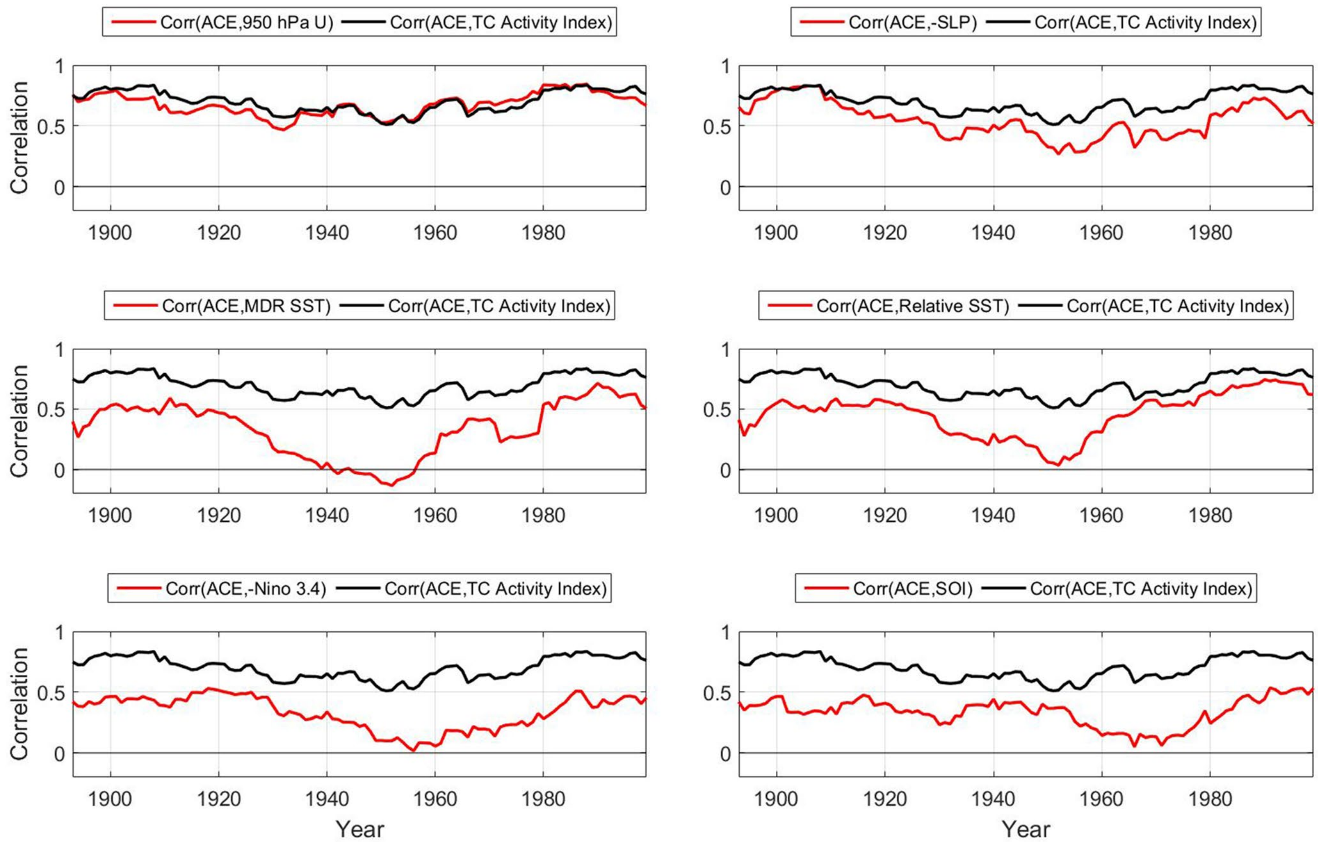

Figure 7. As in Figure 6 but for time-varying correlations of ACE with the Activity Index and the six environmental indices.

zonal wind with NTC is systematically lower than the correlation of the Activity Index and NTC from about 1900–1935. Running correlations are also shown for ACE (Figure 7). The results are qualitatively similar to those for NTC. The main difference is the Activity Index does not outperform the 950 hPa zonal wind by as large a margin over the period 1900–1935.

Correlations of NTC and ACE with the Activity Index, $\tilde{R}_{1t}$ and the six Saunders et al. (2017) indices are given in Table 5. For consistency with Figures 6 and 7, a 31-year running mean was removed from each time series before calculating the correlations. The row labeled 1893–1999 is for the full reanalysis period after removing 15 years from each end to avoid "end effects" of the running mean.

The correlations support our conclusion that, overall, the skill of the Activity Index is the highest of all the indices investigated. We note the correlations remain high for the first half of the record from 1893–1947. This is encouraging because data from this period were not used to estimate the weights used to define the Activity Index.

We also reconstructed the simplified Activity Index ($\tilde{R}_{1t}$) from the 20CR ensemble means using the same methodology used to reconstruct the Activity Index. The running correlations of $\tilde{R}_{1t}$ with NTC and ACE (not shown) are almost identical to those of the Activity Index. Correlations of $\tilde{R}_{1t}$ with NTC and ACE are given in Table 5.

One could argue that by removing the low frequency variability from the tropical cyclone and MSLP records, an important and physically-based signal has been thrown away. With this in mind, the correlations were recalculated using the same 10 time series but without prior removal of the 31 year running means. The resulting correlations (Table 6) are slightly higher (by about 0.03) than those calculated from the high pass filtered time series (Table 5). However, the main conclusion is unchanged: the skill of the Activity Index is the highest of all indices investigated in terms of predicting NTC and ACE.

Table 5
Correlations of NTC and ACE With the Activity Index (AI), Its Simplified Form ($\tilde{R}_{1t}$), and the Six Environmental Indices

	AI	$\tilde{R}_{1t}$	950 hPa U	-SLP	MDRSST	RelSST	-Nino	SOI
NTC								
1893–1999	**0.64**	**0.62**	**0.58**	**0.48**	0.24	**0.44**	**0.41**	**0.30**
1893–1947	**0.63**	**0.63**	**0.54**	**0.45**	0.25	**0.46**	**0.44**	0.22
1948–1999	**0.68**	**0.64**	**0.65**	**0.52**	0.24	**0.43**	**0.39**	**0.38**
ACE								
1893–1999	**0.72**	**0.74**	**0.69**	**0.59**	**0.28**	**0.44**	**0.41**	**0.38**
1893–1947	**0.70**	**0.75**	**0.65**	**0.62**	0.23	**0.38**	**0.43**	**0.39**
1948–1999	**0.76**	**0.74**	**0.76**	**0.56**	**0.38**	**0.54**	**0.39**	**0.38**

Note. Correlations are calculated for three periods. Low frequency variability was removed from all time series using a 31 year running mean before calculating the correlations. Correlations significantly different from zero at the 1% significance level are shown in bold. Correlations with significance levels between 1% and 5% are underlined. Correlation significance was calculated allowing for autocorrelation in the time series.

5.2. The Steering Index

The Steering Index was related to the longitude at which storms cross 35°N in Section 4.2. It is natural to ask how well can the Steering Index reconstruct yearly variations in crossing longitude over the last century using MSLP from the 20CR Reanalysis? The first issue that arises in trying to answer this question is that there are significant differences in the Steering Index calculated from the NCEP and 20CR MSLP reanalysis products over their common period 1948–2014. This is reflected in a sample correlation for the two time series of only 0.80. The discrepancy can be explained by differences in MSLP at the more northerly points of the 3×3 pressure grid. The second issue is the 6° westward shift of the median crossing longitude (Figure 5) is small compared to the variability of the crossing longitudes from year to year. (The standard deviation of the seasonal median crossing longitudes is 10° over the period 1948–2014.) It is therefore not surprising that the correlation between the Steering Index calculated from 20CR pressures, and the yearly median crossing longitudes, is low ($\hat{\rho} = 0.24$ for 1948–2014, $\hat{\rho} = 0.10$ for 1901–2014). Neither value is significantly different from zero at the 10% significance level allowing for serial correlation. This implies the Steering Index, as presently defined, is likely not of practical use for seasonal prediction of zonal shifts of TC tracks.

6. Summary and Discussion

In this study we set out to identify linear combinations of gridded MSLP that could be used to reconstruct TC variability for the North Atlantic. In contrast to earlier studies of TC variability that have used indices

Table 6
As in Table 5 Except That 31 year Running Means Were Not Removed From Any of the Time Series Prior to Calculation of the Sample Correlations

	AI	$\tilde{R}_{1t}$	950 hPa U	-SLP	MDRSST	RelSST	-Nino	SOI
NTC								
1893–1999	**0.66**	**0.63**	**0.63**	**0.43**	**0.40**	**0.51**	**0.37**	**0.26**
1893–1947	**0.63**	**0.60**	**0.56**	**0.47**	**0.43**	**0.55**	**0.44**	0.15
1948–1999	**0.73**	**0.69**	**0.68**	**0.58**	0.27	**0.50**	**0.43**	0.36
ACE								
1893–1999	**0.74**	**0.75**	**0.71**	**0.56**	**0.32**	**0.46**	**0.36**	**0.35**
1893–1947	**0.72**	**0.76**	**0.63**	**0.64**	0.25	**0.37**	**0.40**	0.33
1948–1999	**0.78**	**0.77**	**0.79**	**0.62**	**0.39**	**0.58**	**0.41**	**0.37**

developed for other purposes (e.g., NAO, ENSO), we used TC observations in the definition of our indices. We used a combination of statistical methods (e.g., modified redundancy analysis, cross validation) and physically based reasoning to define the indices over the period 1948–2016.

The Activity Index describes temporal changes in overall TC activity in the North Atlantic basin. It can be well approximated by the sum of two contributions: the pressure gradient across the western subtropical Atlantic that drives the near-surface zonal wind, and the strength and westward extension of the subtropical ridge. The correlation of the Activity Index with NTC using unfiltered data is 0.73 (0.69 using data with the low frequency removed). We showed that the Activity Index, defined by weights estimated from data from 1948 to 2016, has a similar correlation with NTC over the extended period 1878–2014. This provides confidence that the index is not the result of over fitting. We also showed that the index has higher skill over the extended period than the six predictors discussed by Saunders et al. (2017).

The Steering Index describes a zonal shift in TC tracks. It can be well approximated by the sum of two contributions: the pressure gradient along coastal North America from the Gulf of Mexico to eastern Canada, and the strength of the subtropical high in the North Atlantic. We showed that there is a statistically significant westward shift of storm tracks between high and low Steering Index years. However, it was not possible to reconstruct the seasonal mean crossing longitudes using the Steering Index over the extended period. As currently defined, we anticipate the Steering Index will not be useful for operational seasonal forecasting.

Future plans include using our statistical approach to identify modes for seasonal forecasting. This may be attempted initially by predicting the TC occurrences for a given month using lagged MSLP and possibly SST. We also plan to use seasonal forecasts from a coupled atmosphere-ocean model, e.g., the Canadian Seasonal to Interannual Prediction System version 2 (CANSIPSv2) and the European Centre for Medium-Range Weather Forecasts Seasonal Forecast System (SEAS5), as predictors for the modified redundancy analysis. We also intend to investigate the Steering Index on a monthly timescale, as this may lead to more useful information for TC track prediction. In the longer term, our goal is to use such information in support of seasonal forecasting by the Canadian Hurricane Center on a regional scale.

Appendix:

In this section, we outline the approach used to construct a low-dimensional representation of the linear relationship between the gridded TC occurrences and MSLP. The approach leads to the two indices used to predict North Atlantic TC occurrences from large-scale MSLP patterns. It is based on a modified form of redundancy analysis (e.g., Bakalian et al., 2010; Tyler, 1982; von Storch & Zwiers, 2002) to physically interpret covariances between predictors and the responses. Let X denote the $p \times 1$ random vector of predictors and Y denote the $q \times 1$ random vector of responses. Assume X and Y both have zero mean and the following covariance matrix:

$$\mathrm{Cov}\left(\begin{bmatrix} X \\ Y \end{bmatrix}\right) = \begin{bmatrix} \Sigma_{XX} & \Sigma_{XY} \\ \Sigma_{YX} & \Sigma_{YY} \end{bmatrix}$$

Ridge regression (Hastie et al., 2009) of Y on X leads to the following predictor for Y:

$$\hat{Y} = \beta X \tag{1}$$

where

$$\beta = \Sigma_{YX}(\Sigma_{XX} + \alpha^2 I)^{-1}$$

is the $q \times p$ matrix of regression coefficients and α^2 is the ridge parameter. If $\alpha = 0$, the above model reduces to multivariate regression and $\hat{Y}$ is that part of the random vector Y that can be linearly predicted from X by minimizing mean square error (Johnson et al., 2002). Ridge regression is useful when trying to fit a model given highly correlated predictors and a relatively small number of observations (n) compared to predictors

(p). This is the situation we face in the present study. There is however a price to be paid for using the ridge estimator; increasing α^2 shrinks the overall magnitude of the regression coefficients and drives $\hat{Y}$ toward zero. In the present study the regression coefficient matrix β is large ($p \times q$ where $q = 20$ is the number of response variables and $p = 9$ is the number of predictors) and therefore difficult to interpret. One way of reducing the number of predictors, and thus the size of β, is to approximate $\hat{Y}$ using a small number of its principal components as in standard redundancy analysis. More specifically, the $q \times q$ covariance matrix of $\hat{Y}$ is given by:

$$\Sigma_{\hat{Y}\hat{Y}} = \beta \Sigma_{XX} \beta'$$

It has the following spectral decomposition:

$$\Sigma_{\hat{Y}\hat{Y}} = E \Lambda E'$$

where E is a $q \times q$ orthogonal matrix with the q eigenvectors of $\Sigma_{\hat{Y}\hat{Y}}$ as columns, and Λ is a diagonal matrix with the ordered eigenvalues $\lambda_1 \geq \lambda_2 ... \geq \lambda_q$ on the diagonal. The proportion of the total variance of $\hat{Y}$ (i.e., the trace of $\Sigma_{\hat{Y}\hat{Y}}$) accounted for by the first r principal components is $\sum_{i=1}^{r} \lambda_i \,/\, \sum_{j=1}^{q} \lambda_j$ (Johnson et al., 2002). To reduce the number of regression coefficients, we project $\hat{Y}$ onto the first r eigenvectors stored in the $q \times r$ matrix $E_r = \left[e_1\, e_2 \ldots e_r \right]$:

$$\hat{Y}_r = E_r E_r' \beta X = e_1 a_1' X + e_2 a_2' X + \ldots e_r a_r' X \tag{2}$$

where:

$$a_i' = e_i' \beta \qquad i = 1, \ldots, r \tag{3}$$

Each term of the right-hand side of 2 can be thought of as a spatial pattern defined at the response locations (e_i) multiplied by a random amplitude:

$$R_i = a_i' X \qquad i = 1, \ldots, r \tag{4}$$

given by the inner product of X and a spatial pattern (a_i) defined at the predictor locations. We will refer to the R_i as redundancy indices. It is straightforward to show that the redundancy indices are uncorrelated. We will show that, for small r, the physical interpretation of 2 is more straightforward than (1) and leads to more accurate predictions of TC activity over the North Atlantic. With respect to the implementation of the above statistical method, we note that the TC occurrences for many grid boxes exhibit positive skewness. To check the effect of transforming the distribution of the TC occurrences to Gaussianity, we applied a square root transform. Based on visual examination of Q-Q plots (Johnson et al. (2002), results not shown), we concluded that the transform was effective. We then repeated the modified redundancy analysis on the transformed data and found it led to negligible changes in the redundancy modes. The main conclusions also remained the same.

Data Availability Statement

The data used in this study are all publicly available from the following sources:

- NCEP Reanalysis 1: https://www.esrl.noaa.gov/psd/data/gridded/data.ncep.reanalysis.surface.html
- 20th Century Reanalysis V2c: https://www.esrl.noaa.gov/psd/data/gridded/data.20thC_ReanV2c.html
- NOAA ERSSTv5: https://www.esrl.noaa.gov/psd/data/gridded/data.noaa.ersst.v5.html
- HURDAT2: https://www.nhc.noaa.gov/data/#hurdat
- AMO Index: https://www.esrl.noaa.gov/psd/data/timeseries/AMO/
- SOI Index: http://www.bom.gov.au/climate/current/soihtm1.shtml

Acknowledgments
Matthew Lee Titus thanks Environment and Climate Change Canada for providing the time to carry out this research. Keith Thompson was supported by National Sciences and Engineering Council of Canada (NSERC) Discovery Grant RGPIN-42414-2013. E. Oliver was supported by NSERC Discovery Grant RGPIN-2018-05,255. P. Klotzbach would like to acknowledge a grant from the G. Unger Vetlesen Foundation. Finally, we thank the three reviewers for their exceptionally thorough and constructive reviews.

References

Bakalian, F., Ritchie, H., Thompson, K., & Merryfield, W. (2010). Exploring atmosphere-ocean coupling using principal component and redundancy analysis. *Journal of Climate*, *23*(18), 4926–4943.

Bell, G. D., Halpert, M. S., Schnell, R. C., Higgins, R. W., Lawrimore, J., Kousky, V. E., et al. (2000). Climate assessment for 1999. *Bulletin of the American Meteorological Society*, *81*(6), S1–S50.

Brennan, J. F. (1935). Relation of May–June weather conditions in Jamaica to the Caribbean tropical disturbances of the following season. *Monthly Weather Review*, *63*(1), 13–14.

Camargo, S. J., & Barnston, A. G. (2009). Experimental dynamical seasonal forecasts of tropical cyclone activity at IRI. *Weather and Forecasting*, *24*(2), 472–491.

Caron, L., Massonnet, F., Klotzbach, P. J., Philp, T. J., & Stroeve, J. (2020). Making seasonal outlooks of Arctic sea ice and Atlantic hurricanes valuable-not just skillful. *Bulletin of the American Meteorological Society*, *101*(1), E36–E42.

Colbert, A. J., & Soden, B. J. (2012). Climatological variations in north Atlantic tropical cyclone tracks. *Journal of Climate*, *25*(2), 657–673.

Compo, G. P., Whitaker, J. S., Sardeshmukh, P. D., Matsui, N., Allan, R. J., Yin, X., et al. (2011). The twentieth century reanalysis project. *Quarterly Journal of the Royal Meteorological Society*, *137*(654), 1–28.

DeMaria, M. (1996). The effect of vertical shear on tropical cyclone intensity change. *Journal of the Atmospheric Sciences*, *53*(14), 2076–2088.

Elsner, J. B., Liu, K., & Kocher, B. (2000). Spatial variations in major U.S. hurricane activity: Statistics and a physical mechanism. *Journal of Climate*, *13*(13), 2293–2305.

Emanuel, K. (2005). Increasing destructiveness of tropical cyclones over the past 30 years. *Nature*, *436*(7051), 686–688.

Fogarty, C. T., & Gyakum, J. R. (2005). A study of extratropical transition in the western north Atlantic ocean, 1963 to 1996. *Atmosphere-Ocean*, *43*(2), 173–191.

Goldenberg, S. B., Landsea, C. W., Mestas-Nuñez, A. M., & Gray, W. M. (2001). The recent increase in Atlantic hurricane activity: Causes and implications. *Science*, *293*(5529), 474–479.

Gray, W. M. (1968). Global view of the origin of tropical disturbances and storms. *Monthly Weather Review*, *96*(10).

Gray, W. M. (1984). Atlantic seasonal hurricane frequency. Part i: El Nino and 30 mb quasi-biennial oscillation influences. *Monthly Weather Review*, *112*(9), 1649–1668.

Gray, W. M. (1984). Atlantic seasonal hurricane frequency. Part ii: Forecasting its variability. *Monthly Weather Review*, *112*(9), 1669–1683.

Gray, W. M., & Klotzbach, P. J. (2014). Why the Atlantic was surprisingly quiet in 2013 (Tech. Rep.). *Department of atmospheric science, Colorado state university, Fort Collins, CO, 80523*. Colorado State University March http://hurricane.atmos.colostate.edu/Forecasts

Hart, R. E. (2011). An inverse relationship between aggregate northern hemisphere tropical cyclone activity and subsequent winter climate. *Geophysical Research Letters*, *38*, L01705. https://doi.org/10.1029/2010GL045612

Hastie, T., Tibshirani, R., & Friedman, J. (2009). *The elements of statistical learning: Data mining, inference, and prediction*. Springer Science & Business Media.

Johnson, R. A., & Wichern, D. W. (2002). Applied multivariate statistical analysis (5[8]). NJ: Prentice hall Upper Saddle River.

Jones, J., Bell, M., & Klotzbach, P. J. (2020). Tropical and subtropical North Atlantic vertical wind shear and seasonal tropical cyclone activity. *Journal of Climate*, *33*(13), 5413–5426.

Kalnay, E., Kanamitsu, M., Kistler, R., Collins, W., Deaven, D., Gandin, L., et al. (1996). The NCEP/NCAR 40-year reanalysis project. *Bulletin of the American Meteorological Society*, *77*(3), 437–471.

Klotzbach, P. J. (2007). Revised prediction of seasonal Atlantic basin tropical cyclone activity from 1 August. *Weather and Forecasting*, *22*(5), 937–949.

Klotzbach, P. J. (2011). A simplified Atlantic basin seasonal hurricane prediction scheme from 1 August. *Geophysical Research Letters*, *38*(16). https://doi.org/10.1029/2011GL048603

Klotzbach, P. J., & Gray, W. M. (2009). Twenty-five years of Atlantic basin seasonal hurricane forecasts. *Geophysical Research Letters*, *36*, L09711. https://doi.org/10.1029/2009GL037580

Klotzbach, P. J., Saunders, M. A., Bell, G. D., & Blake, E. S. (2017). North Atlantic seasonal hurricane prediction: Underlying science and an evaluation of statistical models. *Geophysical Monograph*, *226*, 315–328.

Klotzbach, P. J., Schreck, C. J., III, Collins, J. M., Bell, M., Blake, E. S., & Roache, D. (2018). The extremely active 2017 North Atlantic hurricane season. *Monthly Weather Review*, *146*(10), 3425–3443.

Knaff, J. A. (1997). Implications of summertime sea level pressure anomalies in the tropical Atlantic region. *Journal of Climate*, *10*(4), 789–804.

Knaff, J. A., Seseske, S. A., DeMaria, M., & Demuth, J. L. (2004). On the influences of vertical wind shear on symmetric tropical cyclone structure derived from AMSU. *Monthly Weather Review*, *132*(10), 2503–2510.

Kossin, J. P., Camargo, S. J., & Sitkowski, M. (2010). Climate modulation of North Atlantic hurricane tracks. *Journal of Climate*, *23*(11), 3057–3076.

Kunkel, K. E., Karl, T. R., Brooks, H., Kossin, J., Lawrimore, J. H., Arndt, D., et al. (2013). Monitoring and understanding trends in extreme storms: State of knowledge. *Bulletin of the American Meteorological Society*, *94*(4), 499–514.

Landsea, C. W. (2015). Comments on "monitoring and understanding trends in extreme storms: State of knowledge". *Bulletin of the American Meteorological Society*, *96*(7), 1175–1176.

Landsea, C. W., & Franklin, J. L. (2013). Atlantic hurricane database uncertainty and presentation of a new database format. *Monthly Weather Review*, *141*(10), 3576–3592.

Landsea, C. W., Gray, W. M., Mielke, P. W., & Berry, K. (1994). Seasonal forecasting of Atlantic hurricane activity. *Weather*, *49*(8), 273–284.

Landsea, C. W., Pielke, R. A., Mestas-Nunez, A. M., & Knaff, J. A. (1999). Atlantic basin hurricanes: Indices of climatic changes. *Climatic Change*, *42*(1), 89–129.

Landsea, C. W., Vecchi, G. A., Bengtsson, L., & Knutson, T. R. (2010). Impact of duration thresholds on Atlantic tropical cyclone counts. *Journal of Climate*, *23*(10), 2508–2519.

Mei, W., Xie, S., & Zhao, M. (2014). Variability of tropical cyclone track density in the North Atlantic: Observations and high-resolution simulations. *Journal of Climate*, *27*(13), 4797–4814.

Pielke, R. A., Jr, & Landsea, C. W. (1998). Normalized hurricane damages in the united states: 1925–95. *Weather and Forecasting*, *13*(3), 621–631.

Power, S. B., & Kociuba, G. (2011). The impact of global warming on the southern oscillation index. *Climate Dynamics*, *37*(9–10), 1745–1754.

Ray, C. L. (1935). Relation of tropical cyclone frequency to summer pressures and ocean surface water temperatures. *Monthly Weather Review*, *63*, 10–12.

Saunders, M. A., Klotzbach, P. J., & Lea, A. S. (2017). Replicating annual North Atlantic hurricane activity 1878–2012 from environmental variables. *Journal of Geophysical Research: Atmospheres*, *122*(12), 6284–6297. https://doi.org/10.1002/2017JD026492

Saunders, M. A., Klotzbach, P. J., Lea, A. S., Schreck, C. J., & Bell, M. M. (2020). Quantifying the probability and causes of the surprisingly active 2018 North Atlantic hurricane season. *Earth and Space Science*, *7*(3) e2019EA000852.

Saunders, M. A., & Lea, A. S. (2008). Large contribution of sea surface warming to recent increase in Atlantic hurricane activity. *Nature*, *451*(7178), 557–560.

Snyder, J. (1987). Map projections – A working manual (Vol. 1395). US Government Printing Office.

Tyler, D. E. (1982). On the optimality of the simultaneous redundancy transformations. *Psychometrika*, *47*(1), 77–86.

Vecchi, G. A., & Knutson, T. R. (2008). On estimates of historical North Atlantic tropical cyclone activity. *Journal of Climate*, *21*(14), 3580–3600.

Vecchi, G. A., Zhao, M., Wang, H., Villarini, G., Rosati, A., Kumar, A., et al. (2011). Statistical–dynamical predictions of seasonal North Atlantic hurricane activity. *Monthly Weather Review*, *139*(4), 1070–1082.

Villarini, G., Vecchi, G. A., Knutson, T. R., & Smith, J. A. (2011). Is the recorded increase in short-duration North Atlantic tropical storms spurious?. *Journal of Geophysical Research*, *116*(D10). https://doi.org/10.1029/2010JD015493

Vitart, F., Huddleston, M., Déqué, M., Peake, D., Palmer, T., Stockdale, T., et al. (2007). Dynamically-based seasonal forecasts of Atlantic tropical storm activity issued in June by Eurosip. *Geophysical Research Letters*, *34*, L16815. https://doi.org/10.1029/2007GL030740

von Storch, H., & Zwiers, F. W. (2002). *Statistical analysis in climate research*. Cambridge University Press.

Xie, L., Yan, T., Pietrafesa, L. J., Morrison, J. M., & Thomas, K. (2005). Climatology and interannual variability of North Atlantic hurricane tracks. *Journal of Climate*, *18*(24), 5370–5381.